Dynamic response of highway bridges to moving loads

Autor(en): **Iyengar, K.T. Sundara Raja / Jagadish, K.S.**

Objekttyp: **Article**

Zeitschrift: **IABSE publications = Mémoires AIPC = IVBH Abhandlungen**

Band (Jahr): **30 (1970)**

PDF erstellt am: **28.06.2024**

Persistenter Link: https://doi.org/10.5169/seals-23592

Dynamic Response of Highway Bridges to Moving Loads

Comportement dynamique des ponts-routes sous les surcharges mobiles

Dynamisches Verhalten von Straßenbrücken unter bewegter Last

K. T. SUNDARA RAJA IYENGAR
Professor of Civil Engineering
Indian Institute of Science,
Bangalore

K. S. JAGADISH
Lecturer in Civil Engineering
Indian Institute of Science,
Bangalore

1. Introduction

The Highway bridge is usually considered as a beam while analysing its response to moving loads. This approach neglects the effect of transverse flexibility on the bridge response. A good number of Highway bridges are known to have widths comparable to their spans. The use of beam theory is, therefore, not always satisfactory. The discrepancies of beam theory are especially clear while considering a bridge under eccentric loading. When the load moves along a line away from the centre line of the bridge, the cross-section of the bridge is subjected to torsion in addition to flexure. This behaviour cannot be taken into account by the beam theory. A more rigorous analysis, preferably appealing to plate theory, is then desirable.

Some experimental studies were conducted by PRINCE ALFARO and VELETSOS [1], and WALKER [2], on the influence of transverse flexibility of the bridge on the response to moving loads. They used an aluminium stiffened plate model to represent the beam and slab Highway bridge. A sprung-mass system was devised to simulate the dynamic action of the vehicle. The dynamic distribution effects of the moving load were studied.

The slab bridge and the beam and slab bridge are the two common types of Highway bridges. The slab bridge can be conveniently investigated by idealising it as an isotropic plate. The beam and slab bridge is a more complex structure and the dynamic analysis of such a bridge system has been carried out by ORAN and VELETSOS [3], by treating the bridge as an isotropic plate continuous over the supporting beams. The response under moving loads of

such a structure has been studied utilising the Lagrangian formulation. The equations of motion have been integrated using the Newmark-β procedure. The differences between the beam theory and the plate-over-beams theory have been discussed.

In this paper, the Highway bridge is represented as an orthotropic plate. The analysis can be applied either to slab bridges or to beam and slab bridges. This facility is provided by the fact that the isotropic plate happens to be a special case of the orthotropic plate. It is true that the orthotropic plate analysis is less rigorous in comparison with the plate-over-beams analysis of ORAN and VELETSOS, with reference to beam and slab bridges. Nevertheless, it is known from the literature [4, 5] that the orthotropic plate theory is a reasonable approximation for beam and slab Highway bridges. The orthotropic plate theory also offers certain advantages in the formulation of the bridge response problem. The normal modes of an orthotropic plate are easily analysed and this facilitates the application of the normal mode method in the response analysis.

A satisfactory treatment of the bridge response problem requires the selection of a suitable model to represent the dynamic behaviour of the moving vehicle. A complex three-degree freedom system, incorporating viscous and Coulomb damping mechanisms, has been suggested by HUANG and VELETSOS [6] for Highway bridges treated as beams. This model represents a tractor-trailer combination, the load being applied to the bridge through three axles. When the bridge is considered to be a two-dimensional structure, the representation of the vehicle becomes more complicated. In this case, a complete representation would require the consideration of the lateral rolling effect in addition to the longitudinal pitching effect in the vehicle. Such a representation would further increase the degrees of freedom of the vehicle model. In the following analysis, a simpler representation of the vehicle is preferred, and the vehicle is approximated by a sprung mass. It is believed that a more involved vehicle model may obscure the essential features of the two-dimensional behaviour of the bridge.

2. Analysis

An orthotropic plate, simply-supported at the edges $x=0$ and a and free at the edges $y = \pm b/2$ is now considered (Fig. 1). It is subjected to a moving sprung load of mass M and spring constant k. The plate and the load are assumed to have no damping. The load is considered to be distributed uniformly over a square area of side $2e$. The centre of this square area moves in the x-direction along the line $y=c$. The plate is assumed to be at rest initially.

The deflection of the bridge is denoted by W and the absolute deflection of the sprung mass by z. The deflection of the mass is measured positive down-

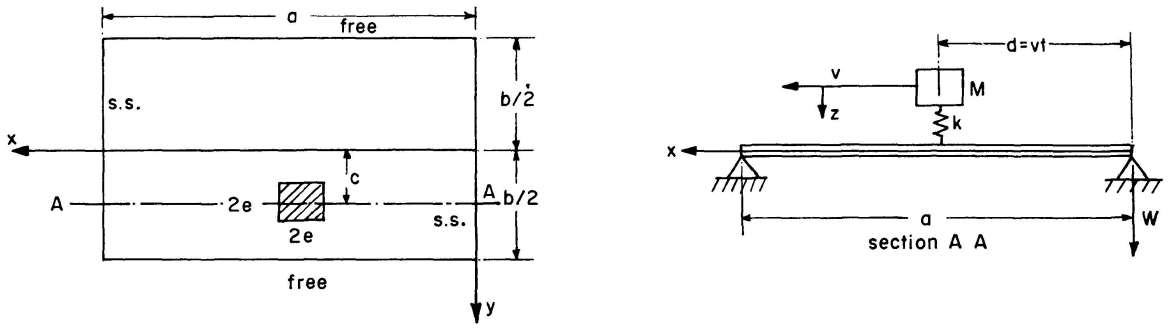

Fig. 1. Orthotropic Plate Under Moving Sprung Load.

wards from its position of equilibrium. The equations of motion of the orthotropic-plate-sprung mass system may be written as follows:

$$D_x \frac{\partial^4 W}{\partial x^4} + 2H \frac{\partial^4 W}{\partial x^2 \partial y^2} + D_y \frac{\partial^4 W}{\partial y^4} + \rho \frac{\partial^2 W}{\partial t^2} = M(g - \ddot{z}) f(x - vt, y) \tag{1}$$

and

$$M\ddot{z} + k[z - W(x, c, t)|_{x=vt}] = 0. \tag{2}$$

M represents the mass of the moving load, D_x, H and D_y are the orthotropic plate rigidities and ρ is the mass of the plate per unit area. f represents the time-dependent function distributing the load over the surface of the bridge. This function is constant over a small area over which the load is considered to be distributed and is zero elsewhere. g is the acceleration due to gravity.

The solution to the Eqs. (1) and (2) can now be obtained by using the characteristic functions of the orthotropic plate. These functions are briefly discussed in the Appendix.

Now the deflection of the orthotropic plate may be expressed as,

$$W = \sum_{m=1}^{\infty} \sum_{n=1}^{\infty} \Phi_{mn}(t) Y_{mn}(y) \operatorname{Sin} \frac{m\pi x}{a}, \tag{3}$$

where $Y_{mn}(y) \operatorname{Sin} \frac{m\pi x}{a}$ represents one of the characteristic functions of the plate and $\Phi_{mn}(t)$ is the corresponding normal co-ordinate. The function $f(x - vt, y)$ may be expressed algebraically as,

$$\begin{aligned} f(x - vt, y) &= \frac{1}{4e^2} \quad \text{if } vt - e < x < vt + e \text{ and } c - e < y < c + e, \\ &= 0 \quad \text{if } x < vt - e \text{ or } > vt + e \text{ and } y < c - e \text{ or } > c + e. \end{aligned} \tag{4}$$

This function can also be expanded by a series as follows:

$$f(x - vt, y) = \sum_{m=1}^{\infty} \sum_{n=1}^{\infty} b_{mn}(t) Y_{mn}(y) \operatorname{Sin} \frac{m\pi x}{a}. \tag{5}$$

Making use of the orthogonal property of the characteristic functions,

$$b_{mn}(t) = \frac{f_{mn}}{K_{mn} a b} \operatorname{Sin} \frac{m\pi vt}{a}, \tag{6}$$

where, $$K_{mn} = \frac{1}{a\,b}\int_0^a \int_{-b/2}^{+b/2} Y_{mn}^2 \operatorname{Sin}^2 \frac{m\pi x}{a}\,dx\,dy$$

and $$f_{mn} = \frac{\operatorname{Sin}\frac{m\pi e}{a}}{\frac{m\pi e}{a}} \frac{1}{2e}\int_{c-e}^{c+e} Y_{mn}\,dy.$$

Making use of (3) and (5) in (1),

$$\ddot{\Phi}_{mn} + p_{mn}^2 \Phi_{mn} = \frac{M(g-\ddot{z})}{a\,b}\frac{f_{mn}}{K_{mn}} \operatorname{Sin}\alpha_m t, \quad \begin{matrix} m = 1, 2 \ldots \\ n = 1, 2 \ldots \end{matrix} \tag{7}$$

where $\alpha_m = \frac{m\pi v}{a}$ and p_{mn} is the circular frequency of vibration of the plate when the shape function happens to be $Y_{mn} \operatorname{Sin}\frac{m\pi x}{a}$. Using (3) in (2),

$$\ddot{z} + \omega^2 z = \omega^2 \sum_{m=1}^{\infty}\sum_{n=1}^{\infty} \Phi_{mn}(t)\, Y_{mn}(c) \operatorname{Sin}\alpha_m t, \tag{8}$$

where $\omega^2 = k/M$.

Eqs. (7) and (8) constitute an infinite set of simultaneous differential equations for the normal co-ordinates $\Phi_{mn}(t)$ and the load displacement z. This set of equations may be solved by numerical means after truncating it suitably. The numerical integration has been carried out by the Runge-Kutta-Nyström method.

The Eq. (3) is found to be inconvenient for the computation of moments due to poor convergence. This difficulty can be surmounted by splitting the solution W into "quasi-static" and "inertia-force" solutions, as indicated below.

Let, $$W(x, y, t) = \overline{W}(x, y, t) + u(x, y, t). \tag{9}$$

$\overline{W}$, represents the quasi-static solution and u represents the inertia force solution. $\overline{W}$ is chosen so as to satisfy the equation,

$$D_x \frac{\partial^4 \overline{W}}{\partial x^4} + 2H \frac{\partial^4 \overline{W}}{\partial x^2 \partial y^2} + D_y \frac{\partial^4 \overline{W}}{\partial y^4} = M(g-\ddot{z}) f(x - v t, y). \tag{10}$$

It is presumed that z is already known by the numerical integration of the Eqs. (7) and (8). $\overline{W}$ then represents the instantaneous static response of the bridge to a moving variable force. This equation can be easily solved by a double series expansion. The quasi-static solution can now be conveniently expressed as,

$$\overline{W}(x, y, t) = \frac{M g}{D_x}\left(1 - \frac{\ddot{z}}{g}\right) a^2 \delta_D, \tag{11}$$

where δ_D is the influence coefficient for deflection at any point (x, y) of the bridge. This influence coefficient is obtained from the solution of Eq. (10) [7].

The coefficient δ_D is only a function of the position of the load and is independent of the speed of the moving load. The moment $\overline{M}_x$ at any point due to the quasi-static solution may be expressed in a similar way as follows:

$$\overline{M}_x(x, y. t) = M g\left(1-\frac{\ddot{z}}{g}\right)\delta_M. \tag{12}$$

δ_M is the influence coefficient for moment at any point.

With $\overline{W}$ defined as above, the function u must satisfy the following equation

$$D_x\frac{\partial^4 u}{\partial x^4}+2H\frac{\partial^4 u}{\partial x^2\partial y^2}+D_y\frac{\partial^4 u}{\partial y^4}=-\rho\frac{\partial^2 u}{\partial t^2}-\rho\frac{\partial^2 \overline{W}}{\partial t^2}=-\rho\frac{\partial^2 W}{\partial t^2}. \tag{13}$$

Making use of (3),

$$D_x\frac{\partial^4 u}{\partial x^4}+2H\frac{\partial^4 u}{\partial x^2\partial y^2}+D_y\frac{\partial^4 u}{\partial y^4}=-\rho\sum_{m=1}^{\infty}\sum_{n=1}^{\infty}\ddot{\Phi}_{mn}Y_{mn}\operatorname{Sin}\frac{m\pi x}{a}.$$

Solving this equation, one can write:

$$u(x, y, t)=-\frac{\rho a b}{D_x}a^2\frac{a}{b}\sum_{m=1}^{\infty}\sum_{n=1}^{\infty}\frac{\ddot{\Phi}_{mn}}{\lambda_{mn}}Y_{mn}\operatorname{Sin}\frac{m\pi x}{a}, \tag{14}$$

where

$$\lambda_{mn}=\frac{\rho p_{mn}^2 a^4}{D_x}.$$

Combining (11) and (14), the complete solution W becomes,

$$W=\frac{M g a^2}{D_x}\left[\left(1-\frac{\ddot{z}}{g}\right)\delta_D-\frac{\rho a b}{M}\frac{a}{b}\sum_{m=1}^{\infty}\sum_{n=1}^{\infty}\frac{\ddot{\Phi}_{mn}}{g\lambda_{mn}}Y_{mn}\operatorname{Sin}\frac{m\pi x}{a}\right]. \tag{15}$$

The bending moment M_x in the orthotropic plate is given by

$$M_x=-D_x\left(\frac{\partial^2 W}{\partial x^2}+\frac{\nu D_y}{D_x}\frac{\partial^2 W}{\partial y^2}\right), \tag{16}$$

where ν is the Poisson's ratio of the slab material. Here, it is assumed that $D_y=D$ where D is the flexural rigidity of the slab of the beam and slab bridge. D_1 is taken to be $\nu D=\nu D_y$ following the analysis of HUFFINGTON [8] for the selection of orthotropic plate rigidities. Applying the above equation to (15),

$$M_x=M g\left[\left(1-\frac{\ddot{z}}{g}\right)\delta_M-\frac{\rho a b}{M}\frac{a}{b}\sum_{m=1}^{\infty}\sum_{n=1}^{\infty}\frac{\ddot{\Phi}_{mn}}{g\lambda_{mn}}\operatorname{Sin}\frac{m\pi x}{a}\left(m^2\pi^2 Y_{mn}-\nu\frac{D_y}{D_x}\frac{a^2}{b^2}\overline{Y}_{mn}\right)\right], \tag{17}$$

where

$$\overline{Y}_{mn}=\frac{b^2 d^2 Y_{mn}}{dy^2}.$$

The values of δ_D and δ_M can be obtained by the static analysis using any routine method [7].

The amplification factors for deflection and moment at midspan can now be expressed as,

Amplification factor for deflection

$$= A F D = \frac{W(a/2, y, t)}{M g a^2 (\delta_D)_{max}} D_x. \tag{18}$$

Amplification factor for moment M_x

$$= A F M = \frac{M_x(a/2, y, t)}{M g (\delta_M)_{max}}. \tag{19}$$

Here $(\delta_D)_{max}$ and $(\delta_M)_{max}$ are the maximum values of the midspan influence coefficients.

3. Numerical Studies

Two typical Highway bridges are considered for detailed numerical study. One of them is a short-span slab bridge and the other is a medium span beam and slab bridge. The geometrical and structural characteristics of the two bridges are summarised in Table 1.

Table 1. Details of Bridges Considered

Bridge Type	Span Metres (Ft.)	a/b	D_x/D_y	$\frac{H}{\sqrt{D_x D_y}}$	$\sqrt{D_x}$ kg$^{1/2}$ m$^{1/2}$ (lb.$^{1/2}$ ft.$^{1/2}$)	ρ kg sec^2/m^3 (lb. sec^2/ft.^{3})	ν
Slab	5.00 (16.41)	1.0	1.0	1.0	2500.00 (6718.75)	60.00 (3.74)	0.0
Beam and Slab	20.00 (65.65)	2.0	100.0	0.4	25,000.00 (67 187.50)	90.00 (5.61)	0.0

In all the numerical results presented here, five modes of the bridge are considered while calculating the inertia-force solution. For these five modes, the value of m is equal to unity and n takes values from 1 to 5. In an earlier study [9], the authors have shown that the bridge response is influenced mostly by the first three modes. The use of five modes in the present case may therefore be considered to be more than adequate. As was mentioned earlier, the Runge-Kutta-Nyström method has been used to integrate the equations of motion. The time interval for the integration has been chosen to be one-tenth the period of the fifth mode in all the calculations.

The entire procedure for numerical integration and the evaluation of amplification factors for deflection and moment was programmed in Fortran to run on a CDC-3600 computer. The programme obtains the ordinates of the amplification history curves at midspan for deflection and moment. It also incorporates a scheme for picking out the peak values of deflection and moment amplifications.

A number of variables, mentioned below, were considered while making a detailed study of the problem.

a) The Speed Parameter

This parameter is given by $\alpha = \frac{v\,T}{2\,a}$ where v is the speed of the moving sprung load and T is the fundamental period of the bridge. The values considered for this parameter lie between 0.06 and 0.20. This range covers most of the practical bridge dimensions and vehicle speeds.

b) The Frequency and Mass Ratios

The frequency ratio is denoted by $\delta_1 = \omega/p_{11}$ and the mass ratio by $\delta_2 = M/\rho a b$. These two ratios are important as they control the oscillation in the sprung load. The practical vehicle frequencies are mostly less than the fundamental frequency of bridges. Accordingly the values of δ_1 between 0.2 and 1.0 are considered. The weight of the vehicle would normally be less than the weight of the bridge even if vehicles in excess of 30 tons are considered. The values of δ_2 between 0.25 and 1.0 are considered in the numerical studies.

c) The Transverse Vehicle Position

This variable is denoted by c. It has a significant influence on the participation of the various modes of the bridge as the load moves over the bridge. In this paper, two values of c i.e. $c = 0.0$ and $0.45\,b$ are considered.

d) Initial Oscillation of the Sprung Load

The initial oscillation of the sprung load can be described by its initial velocity and displacement. A detailed study would require that these two variables should be varied independently. Such an elaborate study was not envisaged in this paper and the initial oscillation is prescribed only by the initial displacement. The initial velocity is taken to be zero for all the calculations. The magnitude of the initial displacement may be conveniently expressed with reference to the static displacement of the spring under load. If z_0 is the initial displacement, then it may be expressed as,

$$z_0 = \delta_3 \frac{M\,g}{k}.$$

Values of $\delta_3 = 0.2$ and 0.75 are considered.

4. Amplification Spectra

The values of AFD_{max} and AFM_{max} at the midspans of the beam and slab bridge are presented in Figs. 2 to 5 for typical loadings against α. Figs. 2 and 3 refer to the beam and slab bridge and the other two figures refer to the slab bridge. The details of these two bridges are given in Table 1.

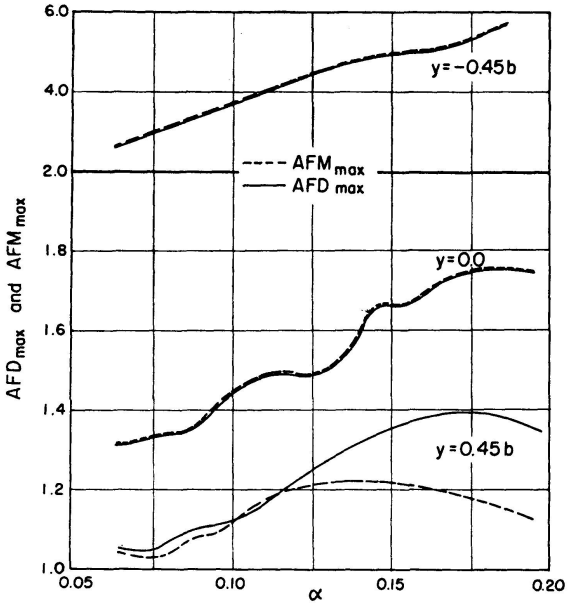

Fig. 2. Amplification Spectra for the Beam and Slab Bridge. Sprung Load Moves Along $y = 0.45b$; $\delta_1 = 0.6$; $\delta_2 = 0.5$; $\delta_3 = 0.0$.

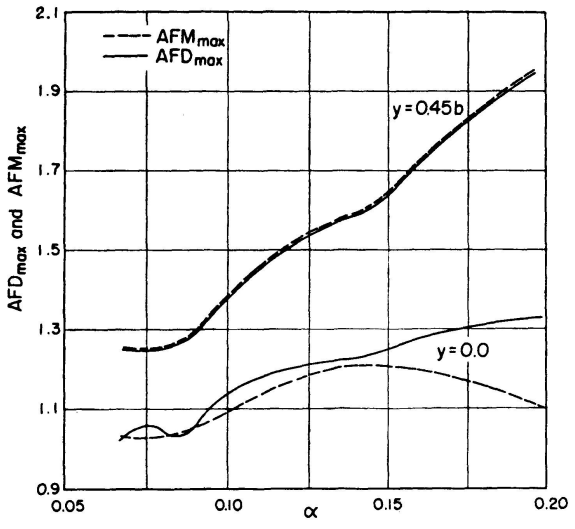

Fig. 3. Amplification Spectra for the Beam and Slab Bridge. Sprung Load Moves Along $y = 0.0$; $\delta_1 = 0.6$; $\delta_2 = 1.0$; $\delta_3 = 0.0$.

Figs. 2 and 3 show the amplification spectra for typical eccentric and concentric loadings respectively, of the beam and slab bridge. The spectra are presented for points at midspan given by $y = \pm 0.45b$ and $y = 0.0$. In general, the amplifications are large for points away from the line of loading. For the midspan point under the loading, the AFM_{max} values are generally smaller than AFD_{max} values. This effect is pronounced for the higher values of the speed parameter. For points away from the line of loading, the AFD_{max} and AFM_{max} values are practically equal. The unloaded edge ($y = -0.45b$) experiences larger amplifications in the eccentrically loaded case than in the concentrically loaded case. However, these large amplifications are not serious, since the static values at the unloaded edge would be quite small due to the nature of the load distribution.

Typical cases of eccentric and concentric loading of the slab bridge are studied in Figs. 4 and 5. All the characteristics noticed in the beam and slab bridge are to be found in this bridge as well. The magnitudes of AFD_{max} and AFM_{max} values at the unloaded edges are much smaller for this bridge.

The amplification spectra obtained by beam theory are presented along with the results of the orthotropic plate theory in Figs. 6 and 7. The beam and slab bridge under eccentric and concentric loadings is considered. For purposes of comparison, the midspan points of the beam and slab bridge lying on the lines of loading are considered. The spectra for such points, by the orthotropic plate theory, are plotted along with the spectra obtained by beam theory. The points indicated in the above happen to be the critically stressed points in the bridge. The amplifications at these points would therefore be of interest to the bridge designer.

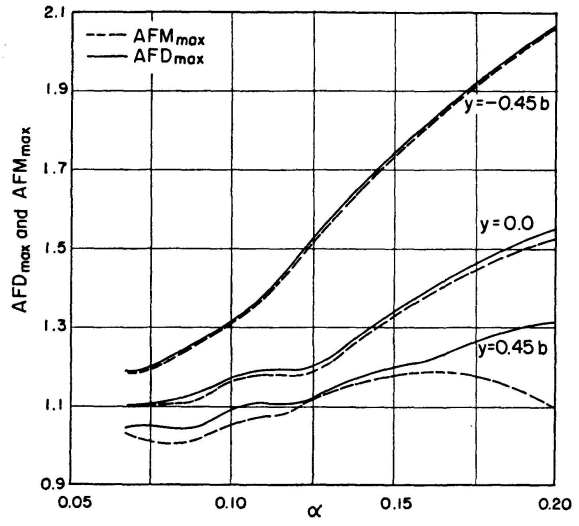

Fig. 4. Amplification Spectra for the Slab Bridge. Sprung Load Moves Along $y = 0.45b$; $\delta_1 = 0.6$; $\delta_2 = 0.5$; $\delta_3 = 0.0$.

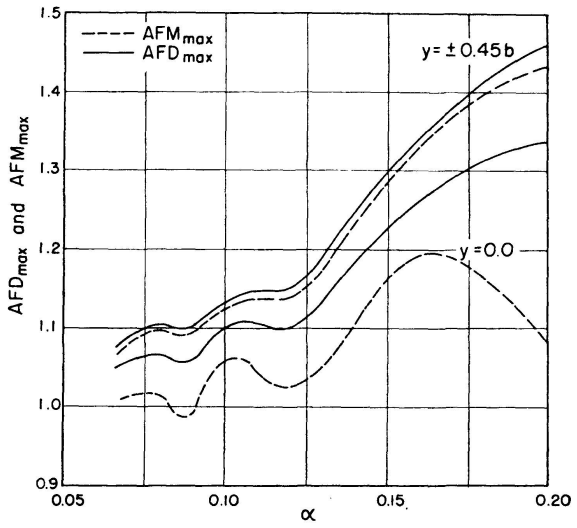

Fig. 5. Amplification Spectra for the Slab Bridge. Sprung Load Moves Along $y = 0.0$; $\delta_1 = 0.6$; $\delta_2 = 0.5$; $\delta_3 = 0.0$.

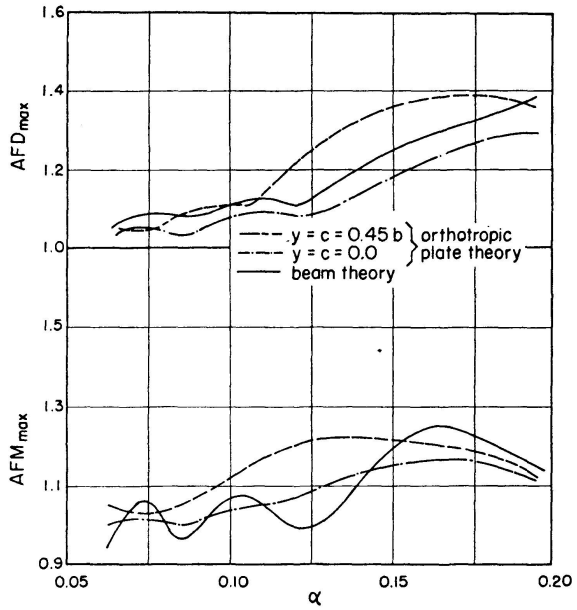

Fig. 6. Comparison of the Spectra by Beam Theory and Orthotropic Plate Theory for the Beam and Slab Bridge. $\delta_1 = 0.6$; $\delta_2 = 0.5$; $\delta_3 = 0.0$.

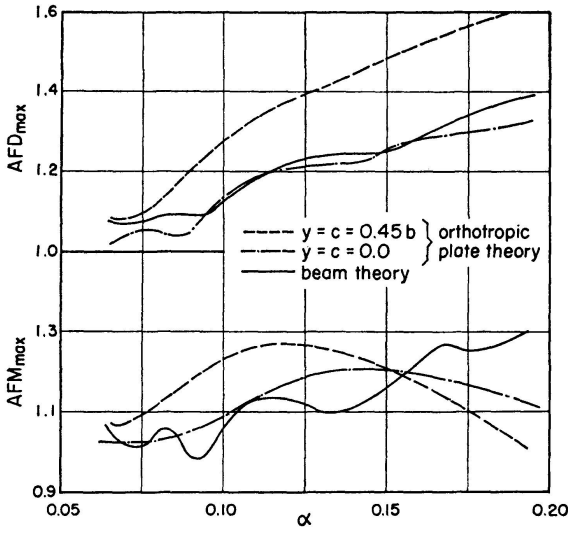

Fig. 7. Comparison of the Spectra by Beam Theory and Orthotropic Plate Theory for the Beam and Slab Bridge. $\delta_1 = 0.6$; $\delta_2 = 1.0$; $\delta_3 = 0.0$.

The shapes of the spectra for AFD_{max} given by the orthotropic plate theory and the beam theory are quite similar. The values of AFD_{max} in the eccentrically loaded case are generally larger than the values given by beam theory. The deflection amplifications for concentric loading are nearly of the same order of magnitude as the amplifications given by beam theory.

There are considerable differences between the shapes of the AFM_{max} spectra given by the orthotropic plate theory and the beam theory. The AFM_{max} values in eccentric loading are larger than the values of the beam theory for the smaller speeds. For the higher speeds, the values by beam

theory are found to be larger than the values in eccentric loading. The magnitudes of AFM_{max} in concentric loading do not differ significantly from the magnitudes found by the beam thory.

A study of a good number of spectral curves [7], besides those presented here, showed that the AFM_{max} for the critically stressed point (i. e. the midspan point in the line of loading) rarely exceeds a value of 1.3, for speed parameter values below 0.2. The study of WALKER and VELETSOS [11] showed that the midspan moment amplification by beam theory does not exceed a value of 1.4 for the same range of speeds. This indicates that the absolute maximum value of the moment amplification given by the beam theory is slightly on the conservative side with reference to the critically stressed point of the Highway bridge. The same conclusion was also obtained by the detailed studies conducted at the University of Illinois [12] on multigirder bridges.

5. The Effect of Mass and Frequency Ratios

The maximum amplification factors for the midspan moment in the slab bridge for eccentric and concentric loadings, are presented in Figs. 8 and 9, as functions of the frequency ratio. The values of α equal to 0.174 and 0.126 are considered. The larger values of AFM_{max} at points on the line of loading, are experienced for δ_1 between 0.6 and 1.0. The same trend is found in beams

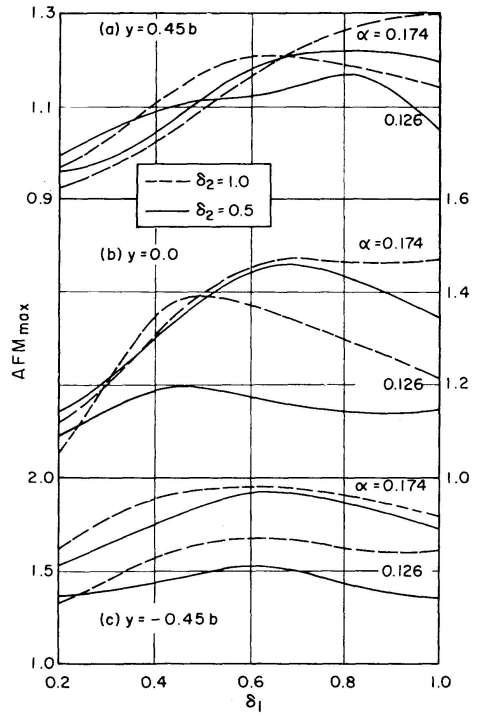

Fig. 8. Influence of Frequency and Mass Ratios on the Maximum Moment Amplification at Midspan. Slab Bridge Under Eccentric Loading. Load Along $y = 0.45b$.

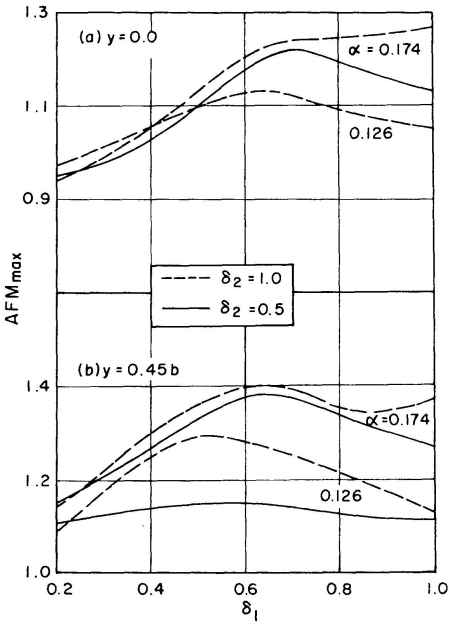

Fig. 9. Influence of Frequency and Mass Ratios on the Maximum Moment Amplification at Midspan. Slab Bridge Under Concentric Loading. Load Along $y = 0.0$.

as observed by WALKER and VELETSOS [11]. When the slab bridge is loaded eccentrically, the unloaded edge is not influenced noticeably, by a change in δ_1. The point $y = 0.0$ at midspan, for eccentric loading, shows increased dynamic effects for δ_1 between 0.6 and 1.0 (Fig. 8), when the speed parameter is 0.174. When the speed parameter is 0.126, the AFM_{max} values at the same point are larger for δ_1 between 0.4 and 0.6. Thus, the figure shows that there can be no simple relationship between the frequency ratio and the maximum amplification factor. The speed parameter affects the instant of bottoming of the sprung load, and this is responsible for the complexity in the dependence of AFM_{max} on δ_1. The same trends are observed even in the concentric loading of the slab bridge (Fig. 9). The effect of mass ratio δ_2 is less pronounced when compared to the frequency ratio. The AFM_{max} values are generally larger for the higher mass ratio, except when δ_1 is small. For the smaller values of δ_1, the mass ratio does not have any noticeable influence.

The detailed studies conducted by JAGADISH [7] showed that similar effects are present in the beam and slab bridge as well.

6. History Curves

The history curves presented here show the variation of AFM and AFD, at certain points, as the sprung load moves over the bridge. Figs. 10 to 13 show some of the typical history curves. The AFM variations for the midspan points $y = \pm 0.45b$ and $y = 0.0$ are plotted in these curves and the AFD variation is shown only for the midspan point in the line of loading. The AFD values were found to be practically equal to the AFM values for points away from the loading. The force of interaction between the sprung load and the bridge is also presented with each graph. This interaction force is represented by $R = Mg(1 - \frac{\ddot{z}}{g})$. All the curves are presented for a speed parameter value of 0.174.

Figs. 10 and 11 show the history curves for the eccentric loading of the beam and slab bridge. In Fig. 10, $\delta_1 = 0.2$ and the unloaded edge shows a beating type of motion. The earlier studies of the authors [7, 9] had shown that the unloaded edge of this beam and slab bridge shows a beating motion as a constant force moves along one of the edges. In Fig. 10, the interaction force R does not vary within wide limits since δ_1 is well below unity. As such, the moving constant force effect may be expected to dominate the response. As the frequency of the sprung load is increased to make $\delta_1 = 0.6$ (Fig. 11), the oscillation of the load becomes more pronounced. The interaction force reaches a value as large as 2.3 Mg when the load is near the third quarter point. The oscillation of the load now interferes with the beating phenomenon at the unloaded edge. When the load is near the third quarter point, the mass bottoms and the negative peaks of the motion of the unloaded edge are reduced in

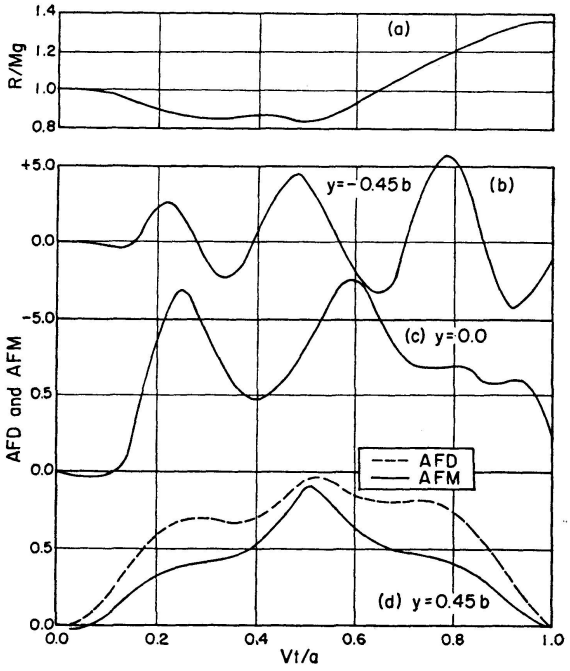

Fig. 10. History Curves for Interaction Force and Midspan Amplifications. Beam and Slab Bridge Under Eccentric Load. Load Along $y = 0.45b; \alpha = 0.174; \delta_1 = 0.2; \delta_2 = 1.0; \delta_3 = 0.0$.

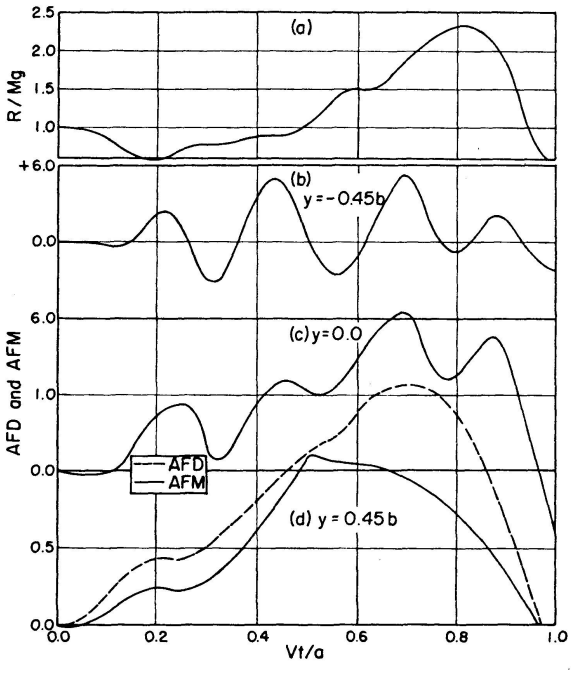

Fig. 11. History Curves for Interaction Force and Midspan Amplifications. Beam and Slab Bridge Under Eccentric Load. Load Along $y = 0.45b; \alpha = 0.174; \delta_1 = 0.6; \delta_2 = 1.0; \delta_3 = 0.0$.

magnitude. In spite of the sharp bottoming near the third quarter, the maximum moment at midspan of the loaded edge occurs when the load is at midspan. However, the moment at midspan remains quite large as the load moves from midspan to the third quarter point. The maximum deflection at midspan of the loaded edge occurs when the load has moved away from midspan. The same feature was observed [9] in the moving constant force problem. It is thus seen that the maximum moment and the maximum deflection at midspan of the loaded edge do not occur at the same instant. This may be explained by the fact that the static influence line for the midspan moment is highly peaked near midspan (for the midspan point on the line of loading) and this causes the maximum dynamic moment to occur when the load is at midspan. The influence line for midspan deflection, on the other hand, is relatively flat near midspan, and the inertia effects may cause the maximum dynamic deflection to occur when the load is away from midspan. This also explains the considerable differences between the AFD_{max} and the AFM_{max} spectra for the loaded edge shown in Figs. 2 and 4. Large values of dynamic deflection can be expected even when the load bottoms well away from midspan. For a large dynamic moment to occur at midspan of the loaded edge, the load must bottom when it is at midspan.

Fig. 12 shows the history curve for the slab bridge under eccentric loading, with $\delta_1 = 0.6$ and $\delta_2 = 1.0$. The unloaded edge of this bridge does not show as large AFM values as were found in the beam and slab bridge. This difference in the behaviour of the two bridges may be attributed to the nature of their

Table 2. Frequencies of Bridges Considered

Type	Frequencies in cycles/sec.			
	Fundamental	I Asymmetric	II Symmetric	II Asymmetric
Slab	20.27	36.73	80.57	159.3
Beam and Slab	10.34	12.09	18.98	33.88

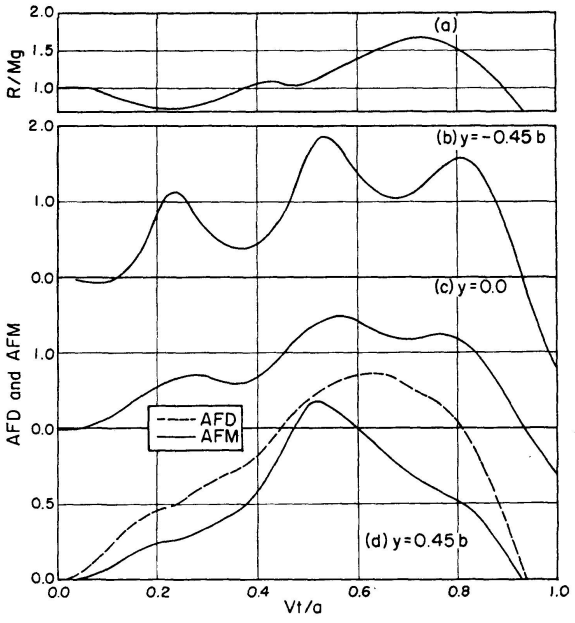

Fig. 12. History Curves for Interaction Force and Midspan Amplifications. Slab Bridge Under Eccentic Load. Load Along $y = 0.45b$; $\alpha = 0.174$; $\delta_1 = 0.6$; $\delta_2 = 1.0$; $\delta_3 = 0.0$.

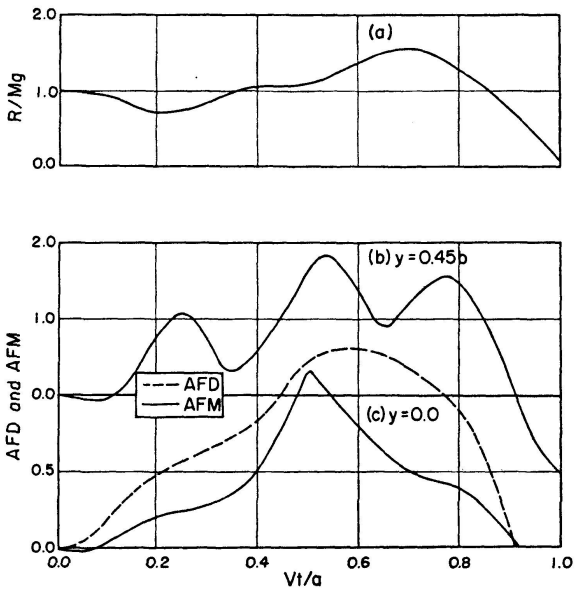

Fig. 13. History Curves for Interaction Force and Midspan Amplifications. Beam and Slab Bridge Under Concentric Load. Load Along $y = 0.0$; $\alpha = 0.174$; $\delta_1 = 0.6$; $\delta_2 = 1.0$; $\delta_3 = 0.0$.

frequency spectra. Table 2 shows the values of the frequencies of the first four modes of the bridges. It is clear that there is a relatively dense distribution of frequencies in the beam and slab bridge. This is especially true of the first two frequencies. Consequently, there is a significant participation by the second mode in the response of the beam and slab bridge.

The history curves for the beam and slab bridge with concentric loading are shown in Fig. 13. The variation in the interaction force is not generally as drastic as it would be for eccentric loading. The differences between the AFD_{max} and AFM_{max} under the load are not so pronounced in this case. The amplification at the points $y = \pm 0.45\,b$ is larger than what is to be found at $y = 0.0$. The maximum moment at the midspan point on the line of loading, is seen to occur when the load is close to midspan.

7. Initially Oscillating Sprung Load

A few history curves for the midspan moment in the beam and slab bridge, with initially oscillating moving load, are presented in Fig. 14 to 16. The

initial oscillation is specified by a positive displacement of the sprung load which is expressed as a fraction δ_3 of the static displacement of the spring under the load. The values of δ_1 and δ_2 are held constant at 0.6 and 1.0 respectively. The parameter δ_3 is given values of 0.2 and 0.75 in these numerical studies.

Figs. 14 and 15 consider the eccentric loading of the beam and slab bridge for speed parameter values of $\alpha = 0.174$ and $\alpha = 0.126$ respectively. The history curves for the case with no initial oscillation are also presented. It is clearly observed that the initially oscillating sprung load undergoes much the same type of oscillation it shows when there is no initial oscillation. The locations

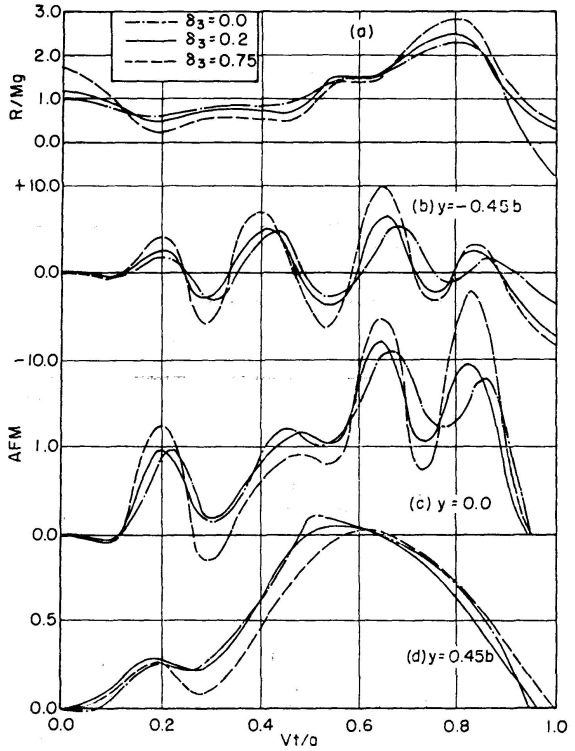

Fig. 14. History Curves for Beam and Slab Bridge Under Eccentric and Initially Oscillating Load. Load Along $y = 0.45b$; $\alpha = 0.174$; $\delta_1 = 0.6$; $\delta_2 = 1.0$.

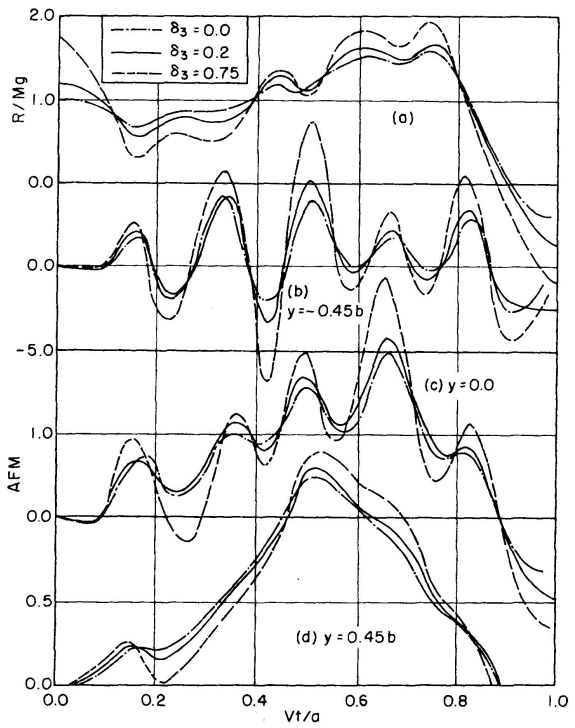

Fig. 15. History Curves for Beam and Slab Bridge Under Eccentric and Initially Oscillating Load. Load Along $y = 0.45b$; $\alpha = 0.126$; $\delta_1 = 0.6$; $\delta_2 = 1.0$.

of the peaks and depressions in the interaction force curve are not shifted as the initial displacement is increased. The amplitudes of the sprung load motion are greater when there is a larger initial displacement. The moment history curves for the different values of initial displacement also follow each other, the oscillations being more violent with the higher value of initial displacement. For $\alpha = 0.174$, a large bottoming of the load occurs, when it is near the third quarter point. As the bottoming occurs well away from midspan, the moment amplification under the line of loading at midspan is not seriously affected by initial oscillation. For midspan points away from the line of loading, the amplitudes of oscillation are affected to a marked degree and the maximum moment

amplifications occur when the load is well away from midspan. With $\alpha = 0.126$, the significant bottoming occurs when the load is nearer midspan. The maximum moment under the line of loading at midspan is therefore considerably influenced by the amplitude of initial oscillation.

Fig. 16 shows the moment response at midspan of the beam and slab bridge under concentric loading, with $\alpha = 0.126$. Features observed for the eccentrically loaded case are repeated here. There is a sharp bottoming of the load when it is at midspan and the increase in initial displacement loads to larger moment at the midspan point on the line of loading.

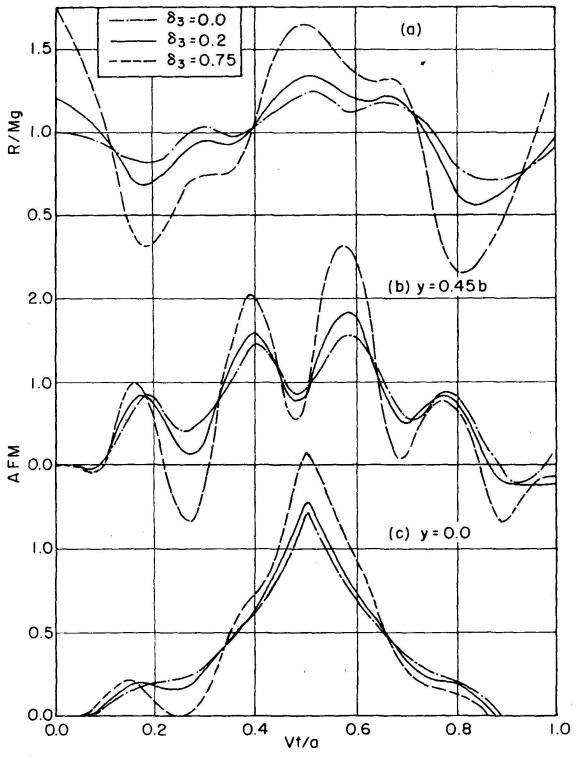

Fig. 16. History Curves for Beam and Slab Bridge Under Concentric and Initially Oscillating Load. Load Along $y = 0.0$; $\alpha = 0.126$; $\delta_1 = 0.6$; $\delta_2 = 1.0$.

8. Transverse Distribution of Dynamic Effects

The transverse distributions of dynamic deflection and moment at midspan, for various positions of the moving load, are shown in Figs. 17 and 18. The beam and slab bridge is considered with $\alpha = 0.174$, $\delta_1 = 0.6$ and $\delta_2 = 0.5$. Initial oscillation is not considered. The distribution of maximum static deflection and moment are shown in dashed lines.

In general, it may be observed that the dynamic profiles do not vary as sharply across the width as the maximum static profiles. This is due to the fact that the maximum dynamic increments of deflection and moment are of the same order of magnitude across the width. This feature of the distribution of dynamic increments was also observed by REILLY and LOONEY [13], in their

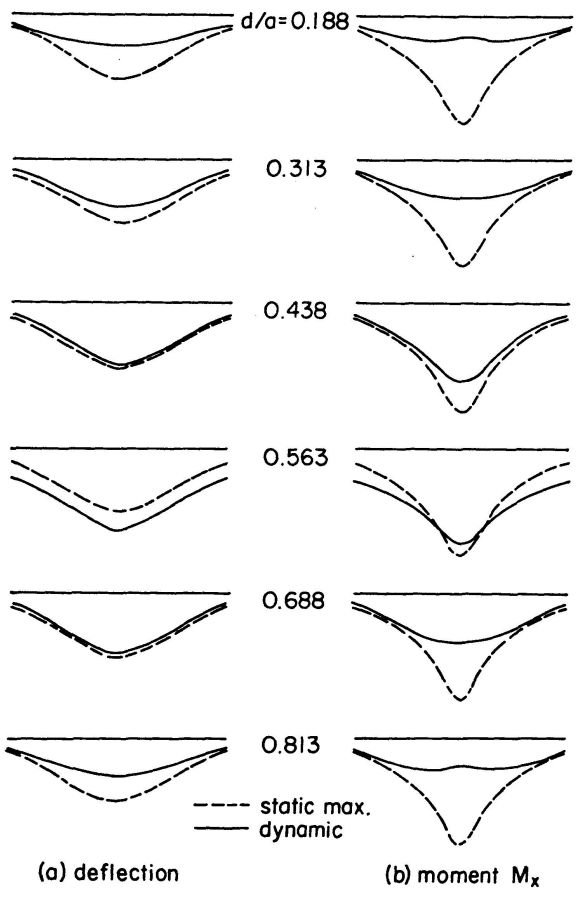

Fig. 17. Transverse Distribution of Dynamic Deflection and Moment at Midspan of the Beam and Slab Bridge. Sprung Load Along $y = 0.0$; $\alpha = 0.174$; $\delta_1 = 0.6$; $\delta_2 = 0.5$; $\delta_3 = 0.0$.

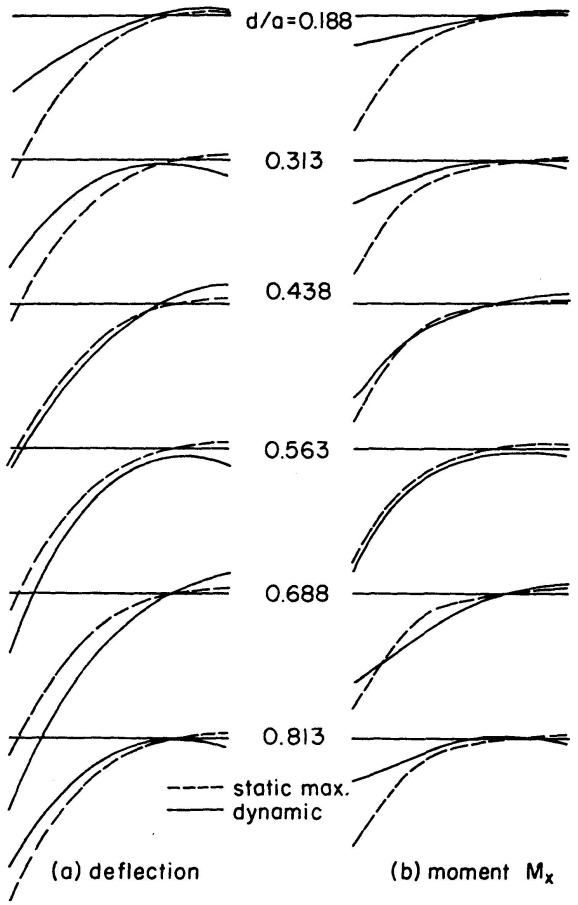

Fig. 18. Transverse Distribution of Dynamic Deflection and Moment at Midspan of the Beam and Slab Bridge. Sprung Load Along $y = 0.45b$; $\alpha = 0.174$; $\delta_1 = 0.6$; $\delta_2 = 0.5$; $\delta_3 = 0.0$.

test results. It may be attributed to the distributing effect of the inertia forces developed in the bridge. In the eccentrically loaded case, the unloaded edge experiences small negative deflections and moments.

9. Conclusions

A study of a large number of results [7], besides those presented here, lead to some general observations about the two dimensional behaviour of Highway bridges. The numerical study was restricted to two typical bridges and this places a limitation on the generality of the conclusions obtained here. However, it is believed that the major trends observed here will be present in most of the other types of beam and slab Highway bridges.

The maximum amplification factors are found to be larger for points in the bridge away from the line of loading. This effect is more pronounced for an eccentrically loaded bridge. In this type of loading, the unloaded edge experiences quite large amplifications irrespective of the frequency and mass ratios.

The amplifications in the beam and slab bridge are much larger than the amplifications in the slab bridge. The amplifications given by the beam theory are slightly on the conservative side when compared to the amplifications of the critically stressed point in the orthotropic plate theory.

For points away from the line of loading, the moment and deflection amplifications are practically equal. For points on the line of loading, the maximum moment amplification factors are generally smaller than the deflection amplification factors. This effect is more pronounced for larger values of the speed parameter. The maximum moment, at the midspan point on the line of loading, always occurs when the load is at or very close to the midspan even if the interaction force is not large at this instant. For the larger values of the speed parameter, the load bottoms near the third quarter point and the maximum deflection amplification occurs when the load has travelled away from the midspan. Thus, the interaction force variation has a stronger influence on the maximum deflection rather than the maximum moment, for points on the line of loading. This accounts for the considerable differences between AFD_{max} and AFM_{max} for such points.

The frequency and mass ratios have definite, although secondary, influences on the response characteristics. When the frequency ratio is between 0.6 and 1.0, large dynamic effects are observed. The effect of mass ratio is less pronounced, although the amplifications generally increase with the mass ratio.

The initial oscillation generally leads to higher amplitude oscillations all over the bridge. The maximum moment, at the midspan point on the line of loading, would be increased significantly by initial oscillation only if the load bottoms at or near the midspan. In a flexible bridge, eccentric loading with initial oscillation may produce pronounced oscillations at the unloaded edge.

Appendix

The expressions for $Y_{mn}(y)$ are presented in this appendix. The functions $Y_{mn}\,\mathrm{Sin}\frac{m\pi x}{a}$ happen to be the shape functions of an orthotropic plate with two opposite edges simply-supported and the other two free. The expressions for the functions may be easily obtained by a free-vibration analysis of the plate.

Modes Symmetric in $y-n$ is Odd

1. $D_1 \neq 0$

$$Y_{mn}(y) = \frac{\mathrm{Cosh}\,\alpha_{mn}\frac{y}{b}}{\mathrm{Cosh}\frac{\alpha_{mn}}{2}} + \frac{\alpha_{mn}^2 - \frac{D_1}{D_y}\frac{m^2\pi^2 b^2}{a^2}}{\beta_{mn}^2 + \frac{D_1}{D_y}\frac{m^2\pi^2 b^2}{a^2}} \frac{\mathrm{Cos}\frac{\beta_{mn} y}{b}}{\mathrm{Cos}\frac{\beta_{mn}}{2}},$$

where α_{mn} and β_{mn} satisfy the equations

$$\tan\frac{\beta_{mn}}{2} = -\frac{\alpha_{mn}}{\beta_{mn}}\left[\frac{\beta_{mn}^2+\frac{D_1}{D_y}\frac{m^2\pi^2b^2}{a^2}}{\alpha_{mn}^2-\frac{D_1}{D_y}\frac{m^2\pi^2b^2}{a^2}}\right]^2\tanh\frac{\alpha_{mn}}{2}$$

and

$$\alpha_{mn}^2 = 2\frac{H}{D_y}\frac{m^2\pi^2b^2}{a^2}+\beta_{mn}^2.$$

2. $D_1=0$

$$Y_{m1}(y) = 1$$

and

$$\beta_{m1} = 0.$$

For values of n greater than unity, expressions of (1) may be used.

Modes Antisymmetric in $y-n$ is Even

$$Y_{mn}(y) = \frac{\operatorname{Sinh}\frac{\alpha_{mn}y}{b}}{\operatorname{Sinh}\frac{\alpha_{mn}}{2}}+\frac{\alpha_{mn}^2-\frac{D_1}{D_y}\frac{m^2\pi^2b^2}{a^2}}{\beta_{mn}^2+\frac{D_1}{D_y}\frac{m^2\pi^2b^2}{a^2}}\frac{\operatorname{Sin}\frac{\beta_{mn}y}{b}}{\operatorname{Sin}\frac{\beta_{mn}}{2}},$$

where α_{mn} and β_{mn} satisfy the equations

$$\tan\frac{\beta_{mn}}{2} = \frac{\beta_{mn}}{\alpha_{mn}}\left[\frac{\alpha_{mn}^2-\frac{D_1}{D_y}\frac{m^2\pi^2b^2}{a^2}}{\beta_{mn}^2+\frac{D_1}{D_y}\frac{m^2\pi^2b^2}{a^2}}\right]^2\tanh\frac{\alpha_{mn}}{2}$$

and

$$\alpha_{mn}^2 = \frac{2H}{D_y}\frac{m^2\pi^2b^2}{a^2}+\beta_{mn}^2.$$

Notation

a, b	Sides of the orthotropic plate.
c	Transverse position of the moving load.
D_1, D_x, H, D_y	Orthotropic plate rigidities.
g	Acceleration due to gravity.
k	Spring constant of the moving load.
M	Mass of the moving load.
p_{mn}	Natural frequency of the orthotropic plate.
R	Force of interaction between the load and the bridge.
v	Speed of the moving load.
W	Deflection of the orthotropic plate.
z	Absolute deflection of the sprung load.
$\alpha=\frac{vT}{2a}$	Speed parameter.

$\alpha_m = \frac{m\pi v}{a}$	Crossing frequency.
$\alpha_{mn}, \beta_{mn}, \lambda_{mn}$	Frequency parameters of orthotropic plate.
$\delta_1 = \omega/p_{11}$	Frequency ratio.
$\delta_2 = M/\rho a b$	Mass ratio.
δ_3	Initial oscillation parameter.
ω	Frequency of the sprung load.
ν	Poisson's ratio of the bridge material.
ρ	Mass per unit area of the orthotropic plate.

References

1. J. Prince Alfaro and A. S. Veletsos: Dynamic Behaviour of an I-Beam Bridge Model under a Smoothly Rolling Load. Eighth Progress Report of the Highway Bridge Impact Investigation, University of Illinois, Urbana, Illinois, October 1958.
2. W. H. Walker: Studies on the Dynamic Response of an I-Beam Bridge Model. Part B, Ninth Progress Report, Highway Bridge Impact Investigation, University of Illinois, Urbana, Illinois, October 1959.
3. C. Oran and A. S. Veletsos: Analysis of Static and Dynamic Response of Simple-span Multi-girder Highway Bridges. Eleventh Progress Report, Highway Bridge Impact Investigation, University of Illinois, Urbana, Illinois, July 1961.
4. C. L. Huang and W. H. Walker: On Free Vibration of Simple-Span I-Beam Bridges. Part D, Ninth Progress Report, Highway Bridge Impact Investigation, University of Illinois, Urbana, Illinois, October 1959.
5. K. T. Sundara Raja Iyengar, K. S. Jagadish and R. Narayana Iyengar: Free Vibration of Beam and Slab Bridges. Journal of the Institution of Engineers (India), Vol. XLVIII, No. 1, Pt. CI 1, September 1967 (Special).
6. T. Huang and A. S. Veletsos: Dynamic Response of Three-Span Continuous Highway Bridges. Structural Research Series No. 190, University of Illinois, Urbana, Illinois, 1960.
7. K. S. Jagadish: The Dynamic Response of Simple-Span Beam and Slab Bridges to Moving Loads. Thesis submitted for the Ph. D. degree, Indian Institute of Science, Bangalore, 1968.
8. N. J. Huffington Jr.: Theoretical Determination of Rigidity Properties of Orthogonally Stiffened Plates. Journal of Applied Mechanics, Vol. 23, p. 15, March 1956.
9. K. T. Sundara Raja Iyengar and K. S. Jagadish: The Dynamic Response of Beam and Slab Bridges to Moving Forces. Publication of the International Association of Bridge and Structural Eng., Vol. 28, No. 2, 1968.
10. C. L. Huang and W. H. Walker: Analysis of Data Obtained from Tests on a Highway Bridge Model. Part D, Tenth Progress Report, Highway Bridge Impact Investigation, University of Illinois, 1960.
11. W. H. Walker and A. S. Veletsos: Response of Simple-Span Highway Bridges to Moving Vehicles. Engineering Expt. Station Bulletin No. 486, University of Illinois, Urbana, Illinois, 1966.
12. A. S. Veletsos: Private Communication.
13. R. J. Reilly and C. T. G. Looney: Dynamic Behaviour of Highway Bridges. Final Report for Maryland State Roads Commission and U.S. Bureau of Public Roads, Civil Engineering Department, University of Maryland at College Park, Maryland, April 1966.

Summary

The response of beam and slab Highway bridges, under the action of moving loads, is studied by the orthotropic plate theory. The moving load is idealised as a mass-spring system. The equations of motion for the problem are solved numerically by the Runge-Kutta-Nyström method. The results are presented in the form of amplification spectra and history curves.

Résumé

On étudie, à l'aide de la théorie des plaques orthotropes, le comportement dynamique des ponts d'autoroutes, formés de dalles ou de poutres. La charge mobile est remplacée par un système de masses sur ressorts. On donne une résolution numérique des équations du problème à l'aide de la méthode de Runge-Kutta-Nyström. Les résultats sont présentés sous forme de spectres d'amplification et de courbes de réponse.

Zusammenfassung

Das dynamische Verhalten von Platten- und Balken-Straßenbrücken unter der Einwirkung bewegter Lasten wird mittels der orthotropen Plattentheorie untersucht. Die bewegte Last wird als ein System federnder Massen idealisiert. Die für das Problem erforderlichen Gleichungen werden numerisch anhand der Runge-Kutta-Nyström-Methode gelöst. Die Resultate werden in Form von Vergrößerungs-Spektren und Hysteresis-Kurven dargestellt.